JOURNAL OF THERMOPHYSICS AND HEAT TRANSFER
Vol. 10, No. 3, July–September 1996

Modeling of Nonequilibrium Radiation Phenomena: An Assessment

Surendra P. Sharma*
NASA Ames Research Center, Moffett Field, California 94035
and
Ellis E. Whiting†
Thermosciences Institute, Moffett Field, California 94035

The present understanding of shock-layer radiation in the low-density regime, as appropriate to hypersonic vehicles, is discussed. Calculated spectra using the NONEQ and GENRAD computer programs are compared with experimental spectra recorded at NASA Ames's electric arc-driven shock-tube facility. The computations predict the intensity of the $N_2^+(1^-)$ system very well, but overpredict the intensities of various atomic O and N transitions and underpredict the intensities of the $N_2(2^+)$ band system. To compute the correct electronic populations, it appears that the quasi-steady-state formulation must be expanded to include more individual electronic states. However, this may cause some computational difficulties and will require excitation rate data for many states, which are not well known.

Nomenclature

$A_{i,j}$ = Einstein transition probability for spontaneous emission, particle^{-1} s^{-1}
B_λ = Planck function, W/cm^2 μm sr
c = velocity of light, cm/s
N = rotational quantum number
N_e = electron number density, cm^{-3}
N_{ion} = ion number density, cm^{-3}
T_e = electron temperature, K
T_{elec} = electronic temperature, K
T_{ex} = excitation temperature, Eq. (1), K
T_R = rotational temperature, K
T_v = vibrational temperature, K
v = vibrational quantum number
α = constant, Eq. (4)
β = constant, Eq. (2)
ε = emission coefficient, W/cm^2 μm sr
κ = absorption coefficient, cm^{-1}

I. Introduction

THE physics of the compressed gas layer behind a shock wave surrounding a hypersonic object flying through a planetary atmosphere has been studied intensely since the early 1960s (Refs. 1–18). The heat generated as a result of the compression is distributed in the shock-layer volume through radiative transport and thermochemical relaxation processes. The translational temperature immediately behind the shock may be as high as 20,000–60,000 K. Because of the high velocity of the vehicle and the low density of the atmosphere, the characteristic flow time through the shock layer becomes comparable to the relaxation time constants of the thermochemical processes and, as a result, a state of thermochemical nonequilibrium exists over a major volume of the shock layer. The radiation from the volume in thermochemical nonequilibrium is enhanced to about 2–15 times its equilibrium value.[16] In such an environment, the nonequilibrium radiation plays a larger role in the radiative heating of the vehicle body. To design the heat shields of such vehicles properly, one must be able to compute the radiative and convective heat load. The convective heat transfer rates can be estimated with confidence, provided the surface catalytic reactivity is known.[19] The nonequilibrium radiation phenomena are still not well understood. Presently, we are able to model and compute,[7] with reasonable accuracy, the radiative emission emanating from shock layers of low-altitude (<50-km) vehicles flying at moderate speeds (6.0 km/s < U_s < 10.0 km/s). However, at higher altitudes (>50 km) and at velocities above 10.0 km/s, the radiative phenomena become very complex and the capability to predict the radiative properties under these conditions is not fully developed.

When chemical and thermodynamic processes in the relaxation zone are binary, i.e., they result from two-body collisions, the intensity of radiation from such reactions is proportional to the density, and the thickness of the relaxation zone is inversely proportional to the density. Consequently, as long as the binary mechanism dominates, the integrated radiation flux emitted from such a nonequilibrium region remains independent of density at a given velocity.[2,3] This property is called the binary scaling law of nonequilibrium radiation.

There are four mechanisms that may depress either the nonequilibrium or equilibrium radiative load to a body, and violate the binary scaling law:

1) Truncation occurs[2] when the width of the nonequilibrium region is thicker than the shock detachment distance.

2) Collisional limiting[8] reduces the radiation intensity at low densities when the collisions are not sufficient to maintain the population of excited states against the depletion by emission.

3) Radiation cooling occurs when energy loss by radiation is significant.

4) Absorption in the gas may occur when the gas is not optically thin.

Electrons play a dominant role in the excitation and emission process. Electrons are about a million times more efficient than neutral particles and a few hundred times more efficient than ions in causing electronic excitations of atoms and mol-

Received Feb. 22, 1994; revision received Dec. 6, 1995; accepted for publication Jan. 3, 1995.

*Senior Research Scientist, M/S 230-2. Associate Fellow AIAA.
†Senior Research Scientist.

ecules by collisions. Furthermore, experiments show[20] that high electronic states, which primarily contribute to the emission, remain in equilibrium with the electrons described by a local Saha equation. Thus, for singly ionized species ($N_e \sim N_{ion}$), the population of excited electronic states is maintained proportional to the square of the electron number density, and hence, so is the spontaneous emission from ionized species. The electrons not only affect the line radiation, but also the continuum radiation. The continuum radiation from free–free emission ($\propto N_e^2$), bound–free recombination processes ($\propto N_e$), and densely packed bound–bound transitions ($\propto N_e^2$), can add up to a significant portion of the total radiative power, especially in an optically thick environment.

There are three basic features that are unique to nonequilibrium radiation:

1) For a given transition, the absorption coefficient κ_λ and the emission coefficient ε_λ must satisfy the principle of detailed balance unique to that particular transition, independently of all other transitions occurring concurrently. The emission coefficient can be expressed as

$$\varepsilon_\lambda = \kappa_\lambda B_\lambda(T_{ex}) \tag{1}$$

Here $B_\lambda(T_{ex})$ is the Planck function dictated by an excitation temperature T_{ex}, defined by the ratio of the upper and lower state populations for the transition. This condition is satisfied whether the gas is in radiative equilibrium or not. If radiative equilibrium exists, the total absorption coefficient, $\kappa_{\lambda t} = \Sigma\, \kappa_\lambda$ and the total emission coefficient $\varepsilon_{\lambda t} = \Sigma\, \varepsilon_\lambda$ are also related by the same excitation temperature. A single excitation temperature cannot be defined in nonequilibrium radiation.

2) During the relaxation process, a state of chemical nonequilibrium exists. The populations of individual radiating species are functions of time (or distance), and must be determined by solving a set of chemical reaction rate equations simultaneously with the thermodynamic and gasdynamic equations.

3) The internal energy distribution for the molecules, as well as the atoms, cannot be determined easily and the populations in individual states are usually defined by assigning individual temperatures.[7,21,22]

While constructing the physical model for the nonequilibrium phenomena features (these features will be discussed in the next section in detail), such as, 1) the use of excitation and radiative transition rate equations for determining the nonequilibrium electronic populations, 2) the quasi-steady-state (QSS) approximation, and 3) the escape factor to account for the absorption and stimulated emission, were used with numerous approximations to simplify the computational effort of the process. During this developmental process, experimental data[1-3,9-15] taken in shock tubes, ballistic ranges, and flight experiments at shock velocities in the range of 6–10 km/s were used to establish the suitability of the models. Laboratory data from shock tubes and ballistic ranges were found most useful for this purpose. Using the models, it was possible to reproduce most of the bulk property data, such as, total radiation intensities, characteristic relaxation times, and the ratio of nonequilibrium-to-equilibrium radiative heat fluxes. However, all attempts to reproduce spectrally resolved emission spectra have been only partially successful.[7,23] Several factors are responsible for this:

1) All previously available experimental data had very poor spectral resolution (AVCO data[1-3] have a resolution of 100 Å).

2) Most of the shock-tube data were distorted by impurities, such as H_2, H_2O, and C in the flow. The extent of these impurities was not usually known and it was difficult to model them.

3) The nature of emission from a shock-heated gas changes with the air enthalpy. For example, at shock velocities lower than 6.0 km/s, heavy particle collisions play a dominant role (e.g., formation of NO), and at moderate velocities (6–9 km/s), electrons play an important role [emission from the $N_2^+(1^-)$ band system]. These phenomena are still not very well understood, particularly when related to individual molecular and atomic transitions.

Now, when the aerospace industry is gearing up to build more efficient launch vehicles with higher than ever re-entry and/or entry velocities, is an excellent time to assess our present capabilities for accurate estimation of nonequilibrium radiation. The spectral details will become important as the operational conditions change, such as at low velocities NO bands become important and in martian atmosphere CN bands and atomic N and O lines become important.

Availability of spectrally resolved spectra (0.5 Å/diode element) from a spectroscopically clean facility at NASA Ames Research Center makes it possible to revisit the nonequilibrium radiation physics with emphasis on spectral details and improve the radiation model. This is the primary motivation behind this article.

In this article, we assess our present capabilities of predicting radiative emission in a low-pressure (0.1 torr) high-speed environment (10.2 km/s). For this assessment, experimental spectra recorded at NASA Ames's electric arc-driven shock-tube facility are compared with calculated spectra. Emission spectra of four species, namely N_2^+, N_2, N, and O, are examined. The discrepancies between the computed and experimental data are discussed to identify weaknesses in the present model. Suggestions for possible ways to improve the present model are also discussed.

II. Physical Model

The present understanding of, and the physical model used to compute, radiative emission from nonequilibrium flows have been discussed in recent publications in great detail.[23–26] However, for completeness, the basic features of the physical model are summarized here. To perform radiation computations one must know the populations in all degrees of freedom of the radiating species as well as their total concentrations. For simplicity, the Boltzmann distributions among the translational, rotational, and vibrational states are specified by assigning individual Boltzmann temperatures for these energy modes. The electron energy distribution is also approximated by an electron temperature. In the fluid flow model the populations in the electronic states are specified by assigning a single electronic temperature to the gas. However, in the radiation model the electronic state populations are computed using the QSS model, described in the next paragraph. In this QSS model each excited electronic state is assigned its own electronic temperature by comparing the population in the state to the population of the ground state. Frequently, for computational simplicity, further approximations such as equating the rotational temperature to the translational temperature and the vibrational temperature to the electron temperature are also made. The total species concentrations are determined by solving fluid flow equations coupled with chemical reaction rate equations.

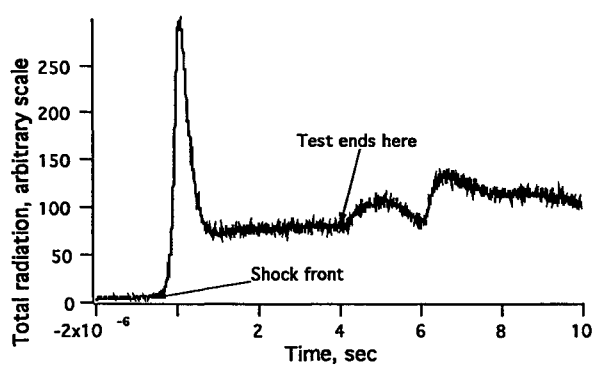

Fig. 1 Total radiation emitted from shock-compressed gas produced in a shock tube. Shock velocity 10.2 km/s in air at 0.1 torr.

A. Radiation Computations

As mentioned in Sec. I, serious errors may result if one computes the radiation based on populations of the electronic states using an effective single electronic temperature. For that reason, the respective electronic state populations are determined from first principles by solving the electronic excitation rate equations. The QSS assumption is valid whenever the excitation and de-excitation rates for any state are both very fast compared to the resultant rate of change of the population of the state. This assumption is usually valid in a shock layer where emission is occurring. Under this assumption the differential excitation rate equations are reduced to linear algebraic equations. To keep the computations within manageable limits, many closely packed electronic levels are often lumped together into effective electronic levels.

Once the electronic state populations are known, as a first step towards computing the radiation, the wavelength of each optical transition is determined. For atomic transitions, this is relatively simple, since the energy levels of the upper and lower levels of each optical transition are explicitly defined. For molecular transitions, the upper and lower energy levels are determined using the vibrational and rotational spectroscopic constants.

The intensities of atomic and molecular lines and continuum radiation are determined differently. For atomic lines the transition probability is given directly in terms of the Einstein A-coefficient. For molecular rotational lines it is given in terms of the product of the electronic transition moment squared, the vibrational Franck–Condon factor, and the rotational line intensity factor. For continuum radiation, the intensities are determined in terms of absorption and emission coefficients. Under equilibrium conditions, the absorption and emission coefficients are related by the Planck function.

For line radiation, the line shape, i.e., the distribution of the transition intensity over wavelength, is required. For most applications, the assumption of a Voigt profile has provided good results with acceptable accuracy.[25] To account for the change in the upper state populations because of absorption and stimulated emission in a complex three-dimensional radiative field in an empirical way, the escape factor is introduced. The es-

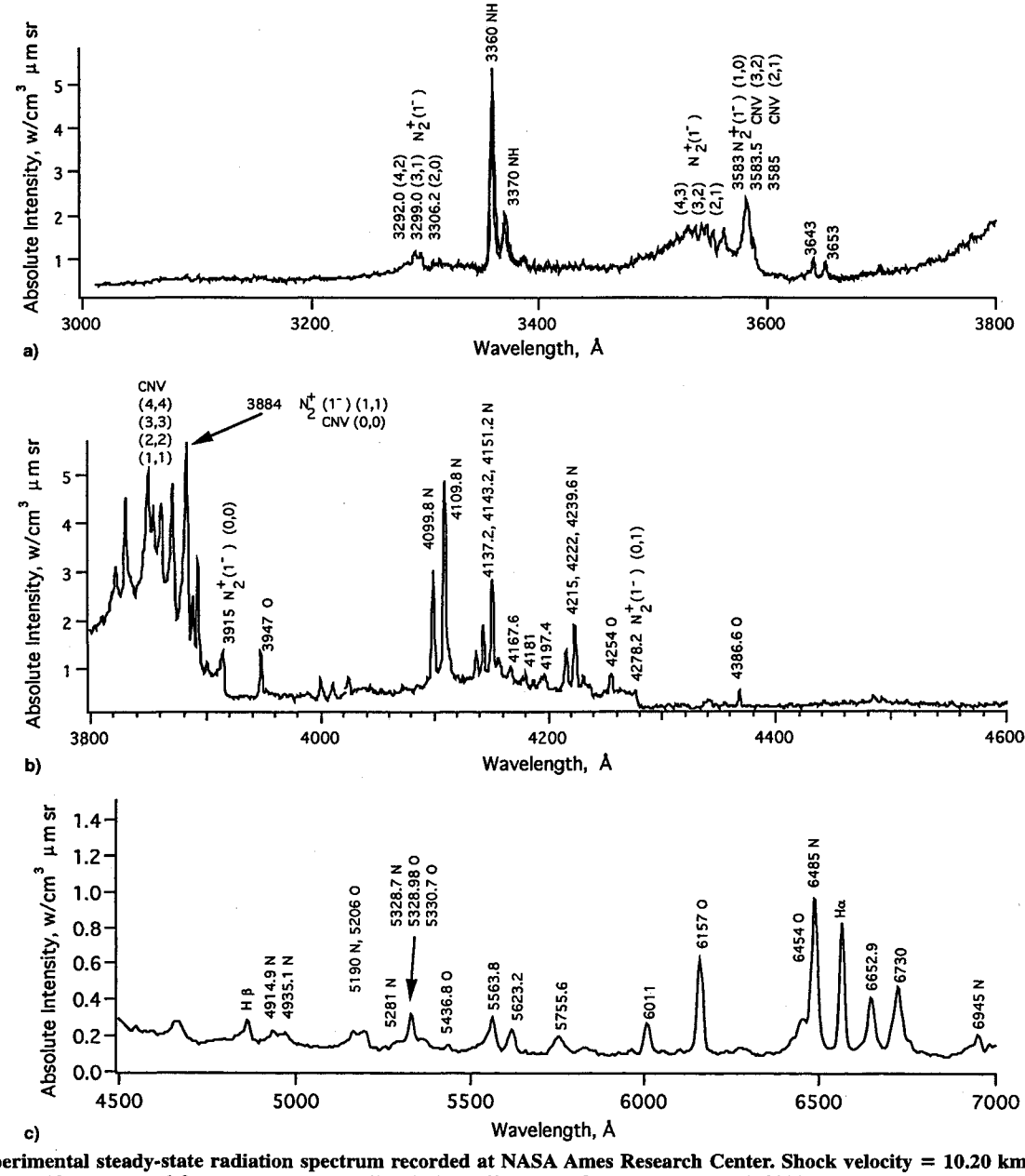

Fig. 2 Experimental steady-state radiation spectrum recorded at NASA Ames Research Center. Shock velocity = 10.20 km/s in 0.1-torr air, image intensifier gate = 1.0 μs, spectrometer slit width = 60 μm, and spectral range a) 3000–3800, b) 3800–4600, and c) 4500–7000 Å.

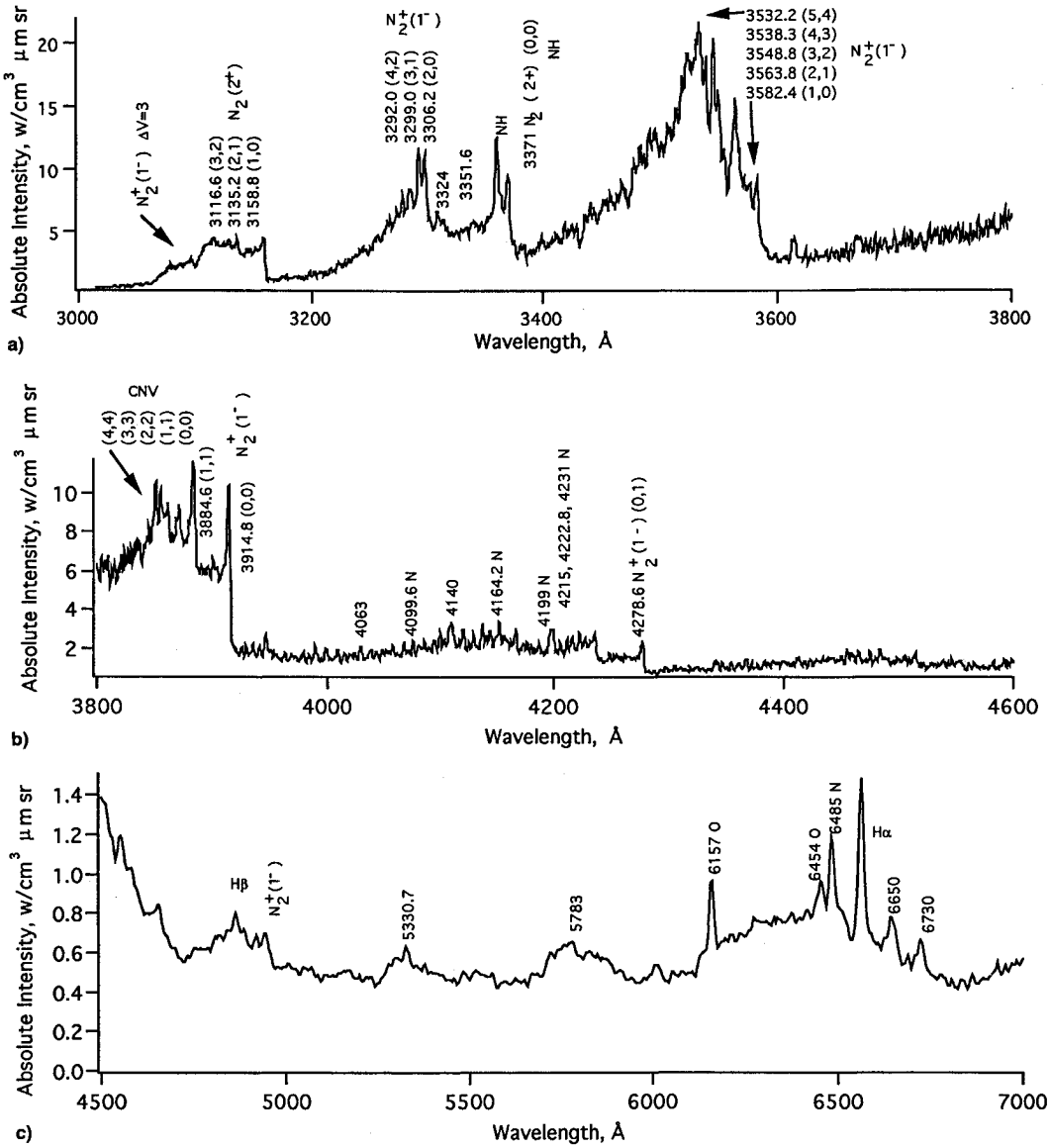

Fig. 3 Experimental nonequilibrium radiation spectrum recorded at NASA Ames Research Center. Point of peak radiation, shock velocity = 10.20 km/s in 0.1-torr air, image intensifier gate = 200 ns, spectrometer slit width = 60 μm, and spectral range a) 3000–3800, b) 3800–4600, and c) 4500–7000 Å.

cape factor accounts for photons that escape from a volume and deplete the upper state populations. It is 1.0 for an optically thin medium, 0.0 for an optically thick medium, and between 0.0–1.0 for an intermediate absorbing medium. The escape factor is approximated from the number density of the absorbing medium, the oscillator strength, the linear size of the emitting volume, and the dispersion line width of the Voigt profile. The line shape is very important in an absorbing medium and radiative heating must be calculated by a radiative transport code.

B. Computation of Species Concentrations

As mentioned previously, the fluid flow equations coupled with the chemical reaction rate equations are solved to determine the species concentrations. For these computations, the electronic temperature is assumed equal to the electron temperature. The effective temperature for rate equations involving both collisions and vibrational energy is written assuming the Park model, $T_a = \sqrt{TT_v}$.

C. Radiation Code

A modified version of Park's[7] NEQAIR program named GENRAD, which incorporates the changes reported in Ref. 26 and several additional features, was used in this research. GENRAD incorporates most of the physics discussed in the previous sections and represents our present understanding of nonequilibrium radiation phenomena. Also, a modified version of Park's code shock-tube radiation program (STRAP), called NONEQ, which combines STRAP, stagnation point radiation program (SPRAP), and GENRAD into a single code and is generalized for any reacting gas mixture, was used to calculate the flow conditions and species concentrations behind the normal shock wave in this study.

III. Experimental Data

The experimental data were recorded at NASA Ames's electric arc-driven shock-tube (EAST) facility.[5] The data were recorded at a shock speed of 10.2 km/s with an initial pressure of 0.1 torr in air. A linear diode array with 700 active elements mounted at the back of a McPherson model 218 0.3-m spectrometer was used to record the spectra. A 1200 lines/mm grating provided a spectral resolution of 0.54 Å per diode element. A radiometer photo-multiplier tube (PMT) was used to record the total radiation from the gases as they passed through the test section (Fig. 1). The figure shows a distinct nonequilibrium overshoot characteristic of this enthalpy regime. After the overshoot

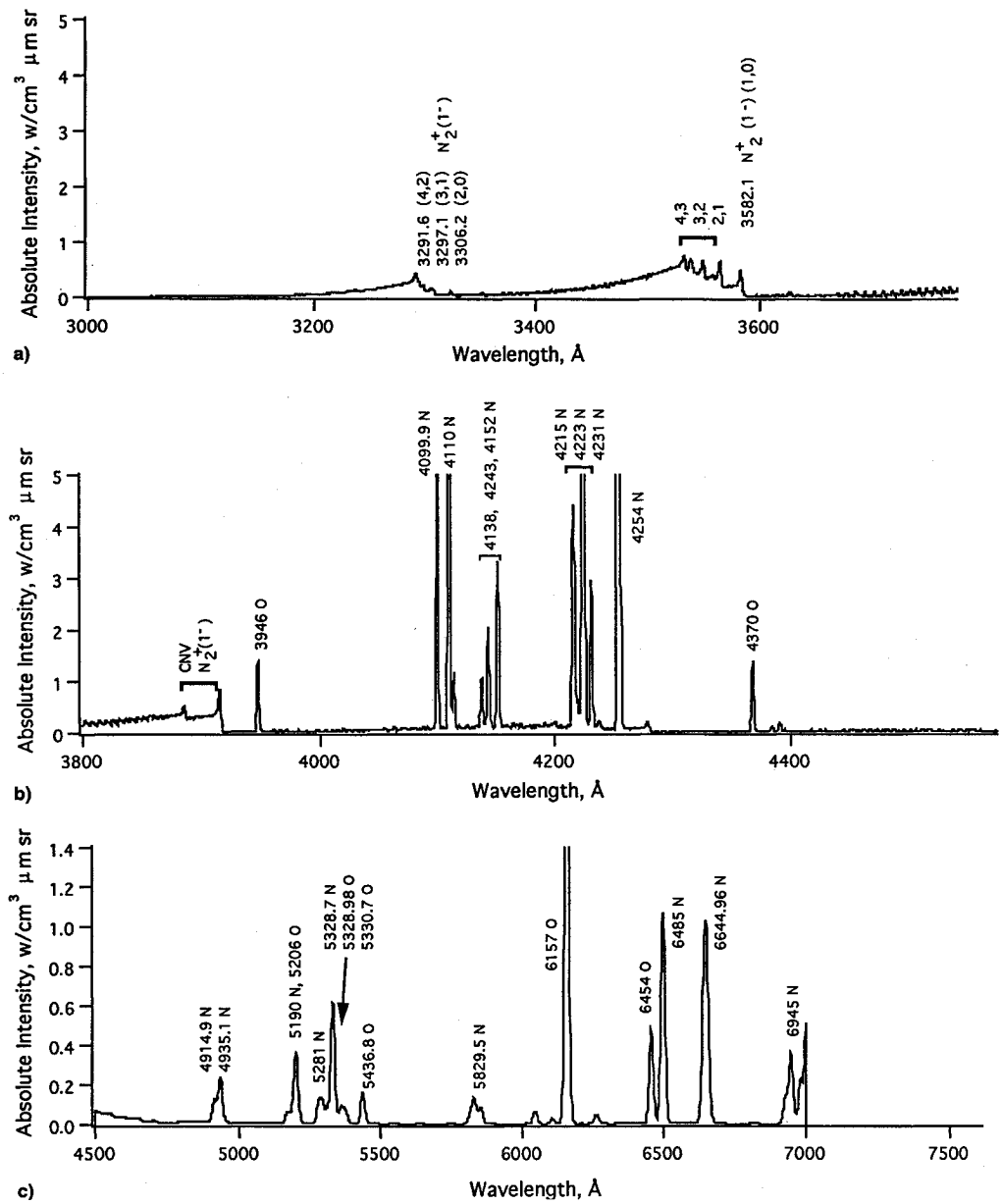

Fig. 4 Computed steady-state spectrum using GENRAD. Spectral range a) 3000–3600, b) 3800–4600, and c) 4500–7000 Å.

the radiation achieves a plateau, which is usually referred to as the equilibrium regime. In fact, as will be clear in the latter part of this article, this regime may not represent a true equilibrium regime and can be best termed as a steady-state regime. In this article, this plateau will be referred to as a steady-state regime.

The total radiation trace in Fig. 1 was used to set the gating of the intensifier placed before the diode array system. For recording the nonequilibrium spectra, the image intensifier to the diode array was activated 50 ns before the peak radiation and left open for 200 ns. For the steady-state spectra, the image intensifier was triggered at about 1.0–2.0 μs after the onset of the peak nonequilibrium radiation (Fig. 1), depending upon the available test time during that run, and was left open for about 1.0–2.5 μs.

The recorded steady-state and nonequilibrium spectra are shown in Figs. 2 and 3, respectively.

IV. Present Model: Theory vs Experiment

The NONEQ code was run to simulate the shock-tube flow with a shock velocity of 10.2 km/s in 0.1-torr room temperature air. The fluid solution coupled with the chemistry provided one-dimensional profiles of species concentrations, translational and vibrational temperatures ($T = T_R$, $T_v = T_e$), and other fluid parameters over a distance of 4.294 cm into the shock-compressed air behind the normal shock front. Air was assumed to be a mixture of 78.087% N_2, 20.950% O_2, 0.93% Ar, and 0.033% CO_2. Nineteen species were considered in the finite rate chemistry solutions, namely: A, C, N, O, C_2, N_2, O_2, CN, CO, NO, CO_2, A^+, C^+, N^+, O^+, N_2^+, O_2^+, NO^+, and electrons. Using the species concentrations, the two temperatures (T and T_v) from the fluid solution, and the electronic populations from the QSS solution, integrated radiative flux spectra for two regions along the axis were computed. The two regions were 1) at t = 0.348–0.525 μs, corresponding to the region of the nonequilibrium overshoot; and 2) at t = 2.17 μs, corresponding to the early portion of the steady-state region; t = 0 corresponds to the location of the shock front.

A. Steady-State Regime

The computed spectra from the steady-state region are shown in Fig. 4. A close comparison with the experimental data (Fig. 2) leads to the following observations:

1. Visible–Infrared Region

1) Calculated N atomic lines are too strong by a factor of 2, O atomic lines by a factor of 4; 2) calculated background too low; 3) H_α at 6560 Å and H_β at 4861 Å in experimental data; 4) NH(0,0) band in second order at 6720 Å in experimental data; and 5) several weak N lines in experimental data, but not in calculation.

2. Ultraviolet Region

1) Calculated atomic N lines from 4100 to 4260 Å are too strong and not in a constant ratio with experiment; 2) calculated atomic O lines at 3946 and 4370 Å are too strong by factors of 2 and 5; 3) calculated $N_2^+(1^-)(0,0)$ bandhead at 3914 Å agrees closely with experiment; 4) the CN–violet bands are much weaker in calculated spectra; 5) strong NH(0,0) band at 3360 Å in experimental data; and 6) unidentified bands at 3830, 3840, and 3895 Å and lines or bands at 3640, 3650, 3960, 4000, 4010, and 4030 Å in the experimental data.

The computed rotational–translational and vibrational temperatures were nearly equal ($T = T_R$ = 10,058 K and $T_v = T_e$ = 10,062 K) and close to the equilibrium temperature (T_{eq} = 10,029 K), indicating a near-equilibrium regime. The species concentration from the finite rate chemistry solutions were in agreement with the equilibrium composition at these temperatures. However, neither of these calculations considered radiative cooling, which is present in the experimental data, although this effect is believed to be small. Thus, high atomic line intensities in the computations are probably not because of a high computed species concentration, but are most likely because of a high upper state population. In other words, the finite rate chemistry model appears to be computing the overall, steady-state species concentrations correctly. Thus, either radiative cooling in the experimental case is lowering the electronic temperature and, hence, the upper state populations, or the QSS electronic excitation subroutine is computing high populations in some electronic states. Computations were also performed with the escape factors set arbitrarily to 1.0 and 0.0, and the results were identical, indicating that the flow is not collisionally limited. Thus, if the problem is with the QSS process, it appears that the excitation rates used may be too high.

The three atomic N multiplets ($^4S° \rightarrow {}^4P$), ($^4P° \rightarrow {}^4P$), and ($^4D° \rightarrow {}^4P$), near 4150, 4220, and 4255 Å, form a single supermultiplet. The energy level diagram for these transitions is shown in Fig. 5. The relative integrated emission of these three multiplets, in equilibrium, are given quite accurately by an L–S coupling theory to be 20:60:100. The calculated intensity ratios, including the effects of absorption (which is negligible in this case), agree with these ratios, but the experimental data clearly do not. Note, however, that the calculated intensities of the $^4S° \rightarrow {}^4P$ multiplet are in good agreement with the experimental data.

The upper states in this case ($^4S°$, $^4P°$, and $^4D°$) all have about the same energy and are all included in the same composite electronic state in the QSS excitation data file. They therefore are assumed to be populated and depopulated at the same rate. Thus, even in the steady-state regime, where the excitation rates should not affect the results, the upper state populations appear to be considerably different from that given by the L–S coupling theory. Clearly, the states are not in equilibrium and it appears that, in this case, the rates for the $^4P°$ and $^4D°$ states are much slower than that for the $^4S°$ state, such that the radiative transition rates are controlling the steady-state populations for these levels.

B. Nonequilibrium Regime

The following observations are made by comparing the computed nonequilibrium spectra (Fig. 6) with the experimental data (Fig. 3):

1. Visible–Infrared Region

1) Calculated atomic line intensities are too strong, the N lines by about a factor of 10, but the O lines by varying amounts; 2) the background is too high below 5000 Å and too low above 5000 Å; and 3) H_α, H_β, and second-order NH are present in the experimental data.

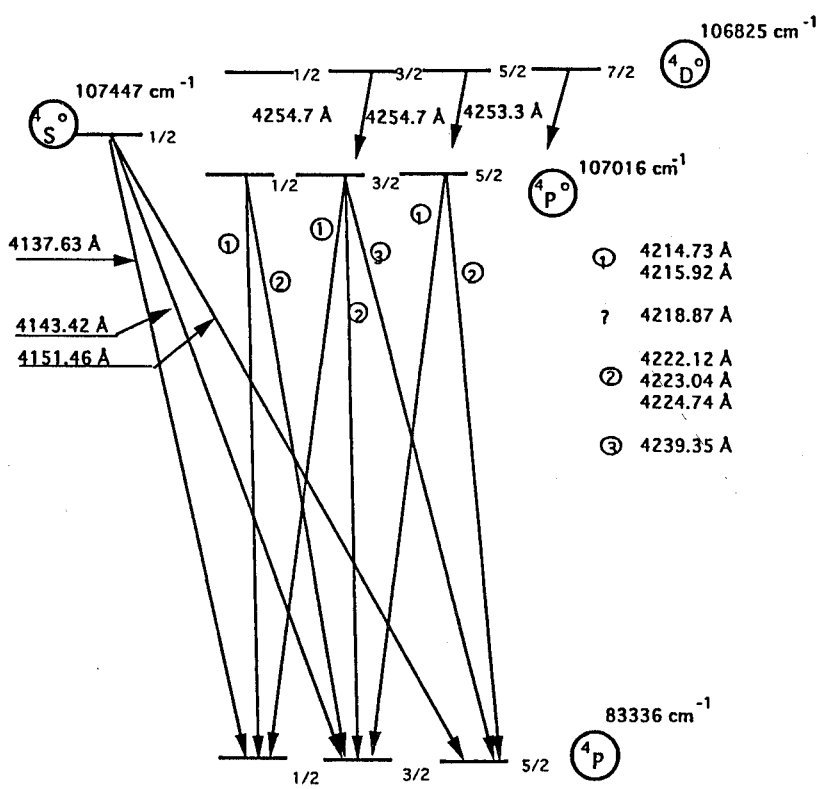

Fig. 5 Super multiplet of atomic nitrogen at 4215–4254 Å (not to scale).

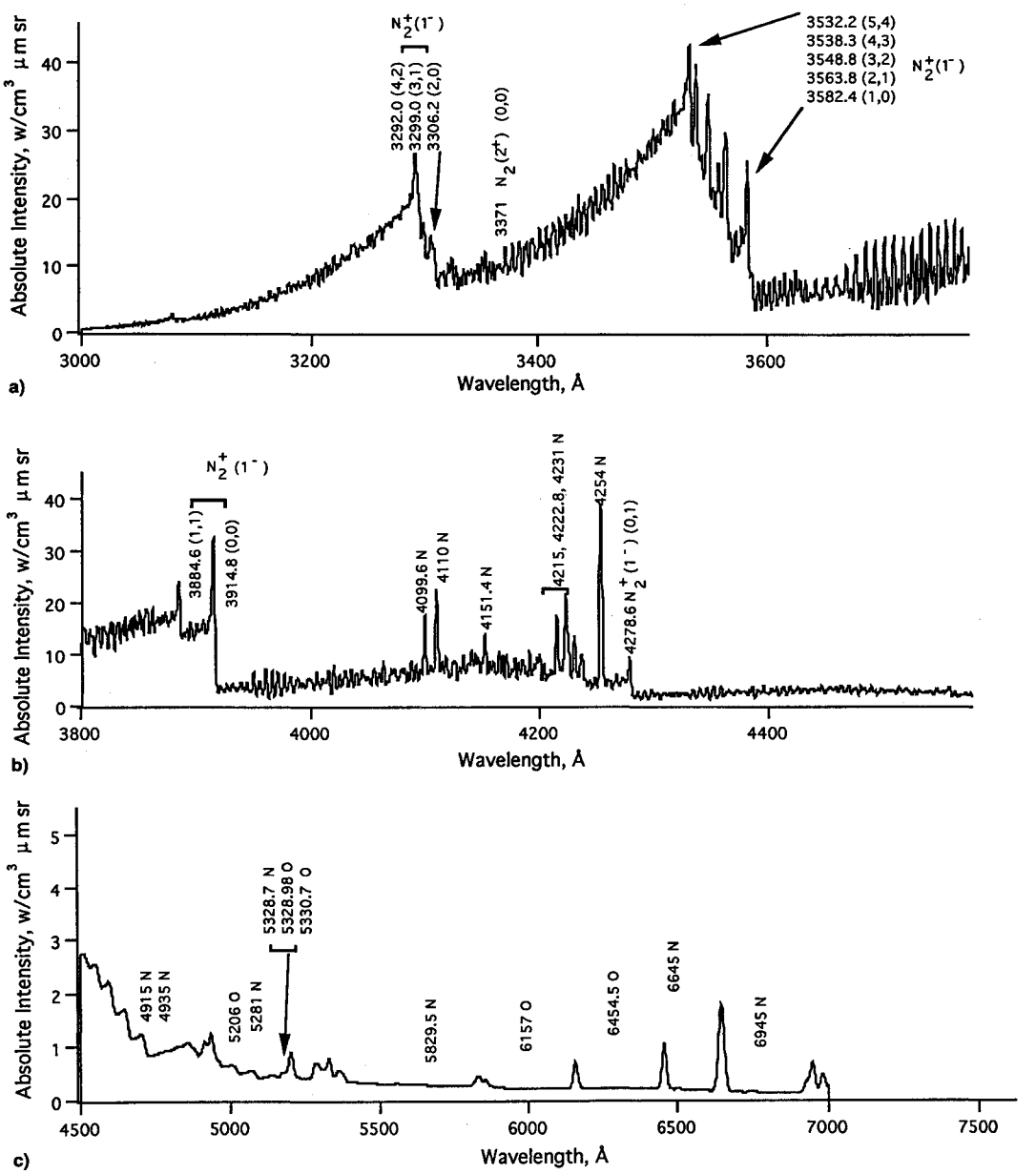

Fig. 6 Computed nonequilibrium spectrum using GENRAD computer code. Point of peak radiation, spectral range a) 3000–3800, b) 3800–4600, and c) 4500–7000 Å.

2. Ultraviolet Region

1) Calculated N lines from 4100 to 4260 are far too strong. These lines do not appear clearly in the experimental data; 2) the calculated $N_2^+(1^-)$ bands are too strong by a factor of 2–3; 3) $N_2(2^+)$ bands are in the data, but in the calculations are too weak to be seen; 4) the experimental (0,0) bandheads for $N_2^+(1^-)$, CN–violet, and $N_2(2^+)$ are all clearly defined; 5) NH (0,0) band at 3360 in the experimental data; 6) the rotational structure of the $N_2^+(1^-)(0,0)$ band in the data shows that the populations of the lower rotational levels are higher than the calculated populations; 7) contrary to the previous item, the shape of the $\Delta v = +1$ sequence of $N_2^+(1^-)$ indicates that the populations of the high rotational levels are less than the calculated populations; and 8) the intensity of the $N_2^+(1^-)(2,1)$ band in the data, relative to the other bands in the $\Delta v = +1$ sequence, indicates that the $v' = 2$ vibrational level may have a high population.

It appears that the populations of various electronic states are not being computed correctly, and also that the population distributions in the rotational and vibrational states show a departure from Boltzmann distributions.

V. Adjustments to Upper State Populations

To visualize the nature and the extent of the discrepancies between the computed and experimental spectra, arbitrary adjustments to the upper state populations were made, until the computed spectra were in close agreement with the experimental data. It should be emphasized that these adjustments were made for illustrative purposes only; to quantify the error in computations in relation to the experimental data. By no means should these adjustments be regarded as the correction factors to the physical models. We postulate that the adjustment factors for each set of experimental data will probably be different. In a different regime the extent of the discrepancies seen here may increase or decrease and/or new spectral regions of discrepancies may appear. However, the conclusions drawn from this adjustment exercise highlight the areas of concern in the physical model, such as QSS formulation, which need attention.

The adjustments to the computations in the present case were primarily applied in the nonequilibrium regime, although some adjustments in the steady-state regime were also required to bring the computed and experimental spectra into general agreement.

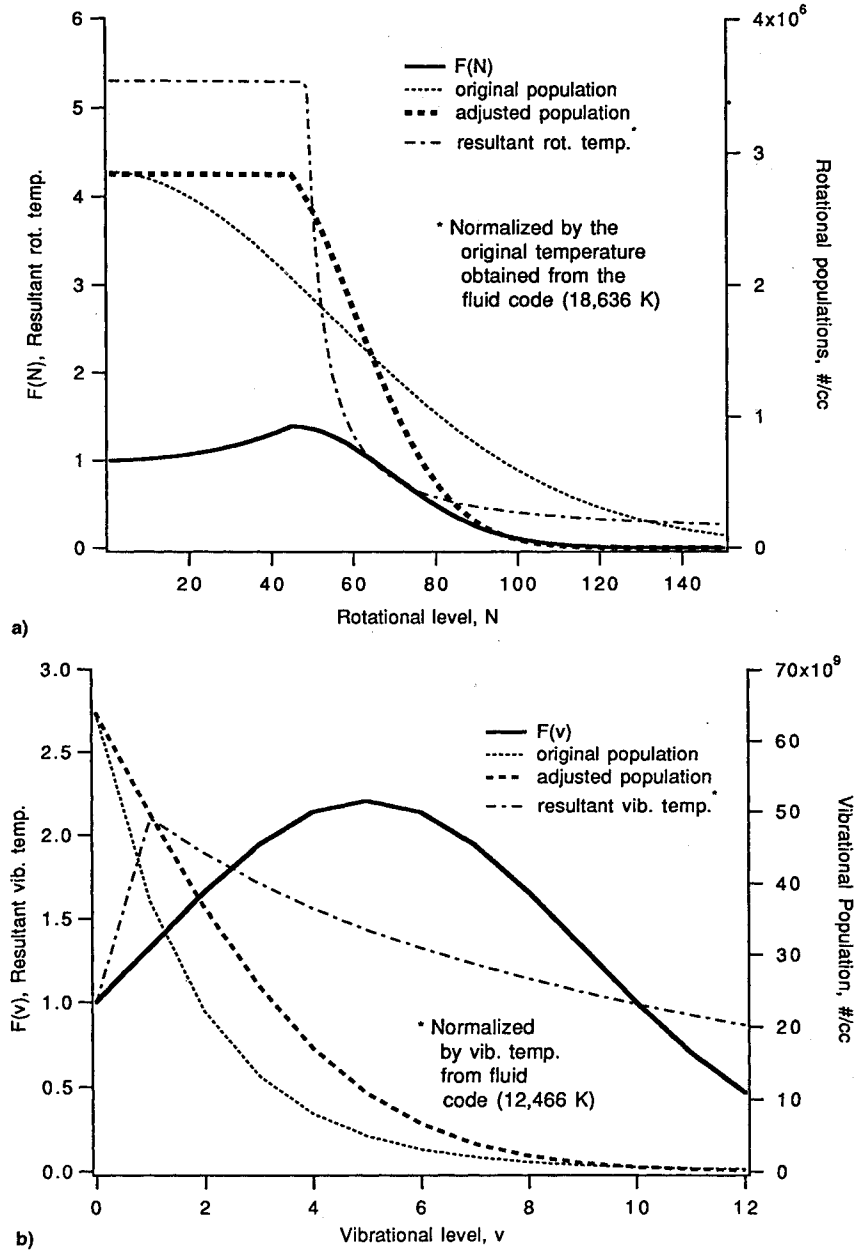

Fig. 7 Adjustment factors. Nonequilibrium radiation for a) rotational and b) vibrational levels.

A. Adjustments

1) Populations of the upper electronic states were adjusted by multiplying by a suitable factor f to simulate a change in the electronic temperature and are used herein to force agreement between the calculated and experimental intensities for atomic lines and the (0,0) molecular bandheads.

2) Relative populations of the vibrational levels of the molecules were adjusted by keeping the $v' = 0$ level unchanged and multiplying the other v' levels by excitation factors $F(v')$, to simulate a change in vibrational temperature. Each vibrational level in an electronic state can have a distinct vibrational temperature.

3) Relative populations of the rotational levels were adjusted by keeping the $N' = 0$ level unchanged and multiplying the other N' levels by excitation factors $F(N')$ to simulate a change in rotational temperature, where each level can have a distinct rotational temperature. The adjusted rotational temperatures are held constant for all vibrational levels in an electronic state.

4) The method of applying the three adjustments described previously is to first adjust the rotational populations to provide the correct shape to the vibrational bands, then the vibrational populations are adjusted to give the correct shape to the vibrational sequences, and lastly the electronic populations are adjusted to match the intensities of the (0,0) bandheads. The reason for this sequence is to maintain realistic vibrational populations as the temperatures are varied so that the sum of all vibrational populations remains equal to the population of the electronic state.

The vibrational population of any given vibrational level is, obviously, the sum of all rotational level populations in that vibrational level. Thus, to maintain a consistent set of populations, a nonequilibrium partition function was developed that used the array of adjusted rotational temperatures calculated from the rotational population distribution.

An exception to the previous sequence was made in the case of the $N_2(2^+)$ band system because the original calculated intensity was too low to be seen in the spectrum. Thus, an initial adjustment of the population of the upper electronic state was made by multiplying by an arbitrary f value of 2000. This value proved to be a lucky choice and it was unnecessary to

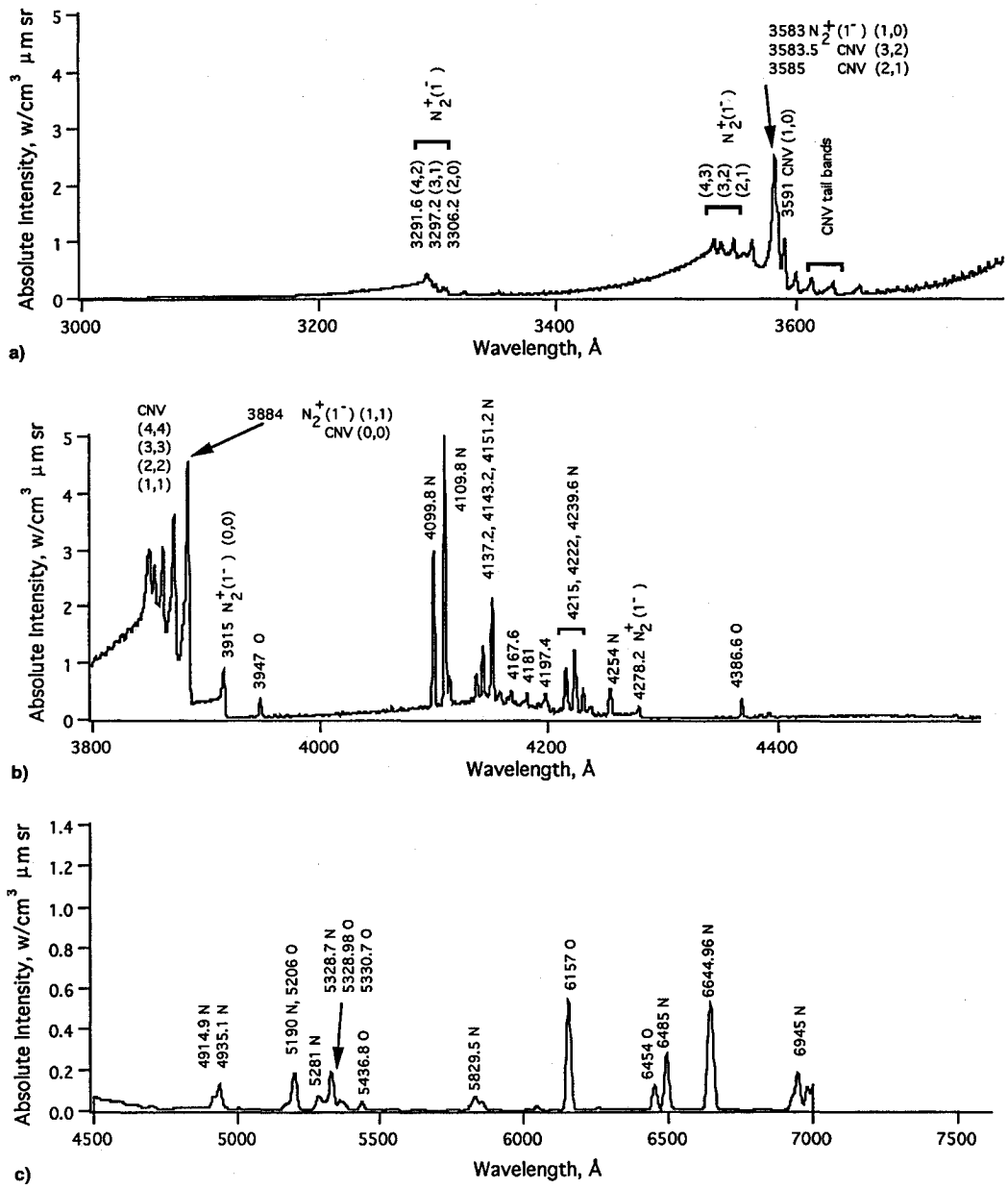

Fig. 8 Adjusted steady-state synthetic spectrum. Spectral range a) 3000–3800, b) 3800–4600, and c) 4500–7000 Å.

adjust it again after the rotational and vibrational populations had been adjusted.

B. Excitation Factors $F(v')$ and $F(N')$

1. Rotational Factor $F(N')$

An empirical expression for the rotational factor was selected to be simple and to conform to the observations made in Sec. IV, that is, a high population in the lower rotational levels and a low population in the high rotational levels. Exploratory calculations indicated that the shape of the $N_2^+(1^-)(0,0)$ band could be matched very well by simply holding the populations of the lower rotational levels equal to the population for the $N' = 0$ level. Such a distribution implies a rotational temperature of infinity, which was arbitrarily set to 100,000 K for use in the calculation of the partition function. The calculations also indicated that the decline in the populations of the high rotational levels had to be very abrupt after some value of N'. Expressions that easily reproduced these effects are shown in Fig. 7. Here, $n(N')$ denotes the actual computed number density in the rotational level N', and $\bar{n}(N')$ is the adjusted value. The expressions stipulate a constant value region

$$\bar{n}(N') = n(0) \quad \text{for} \quad N' \Leftarrow N_p$$

and a rapidly declining region

$$\bar{n}(N') = F(N')n(N') \quad \text{for} \quad N' > N_p$$

where $F(N')$ is given by the Gaussian function:

$$F(N') = F(N_p)\exp[-\beta(N' - N_p)^2] \tag{2}$$

The values entered to specify the Gaussian function are the N' value at the peak of the Gaussian N_p, and the intercept of the Gaussian on the $F(N')$ axis $F(0)$. The $F(N')$ value at the peak of the Gaussian is given by

$$F(N_p) = n(0)/n(N_p) \tag{3}$$

and the value of β is given by

$$\beta = \ell n[F(N_p)/F(0)]/N_p^2 \tag{4}$$

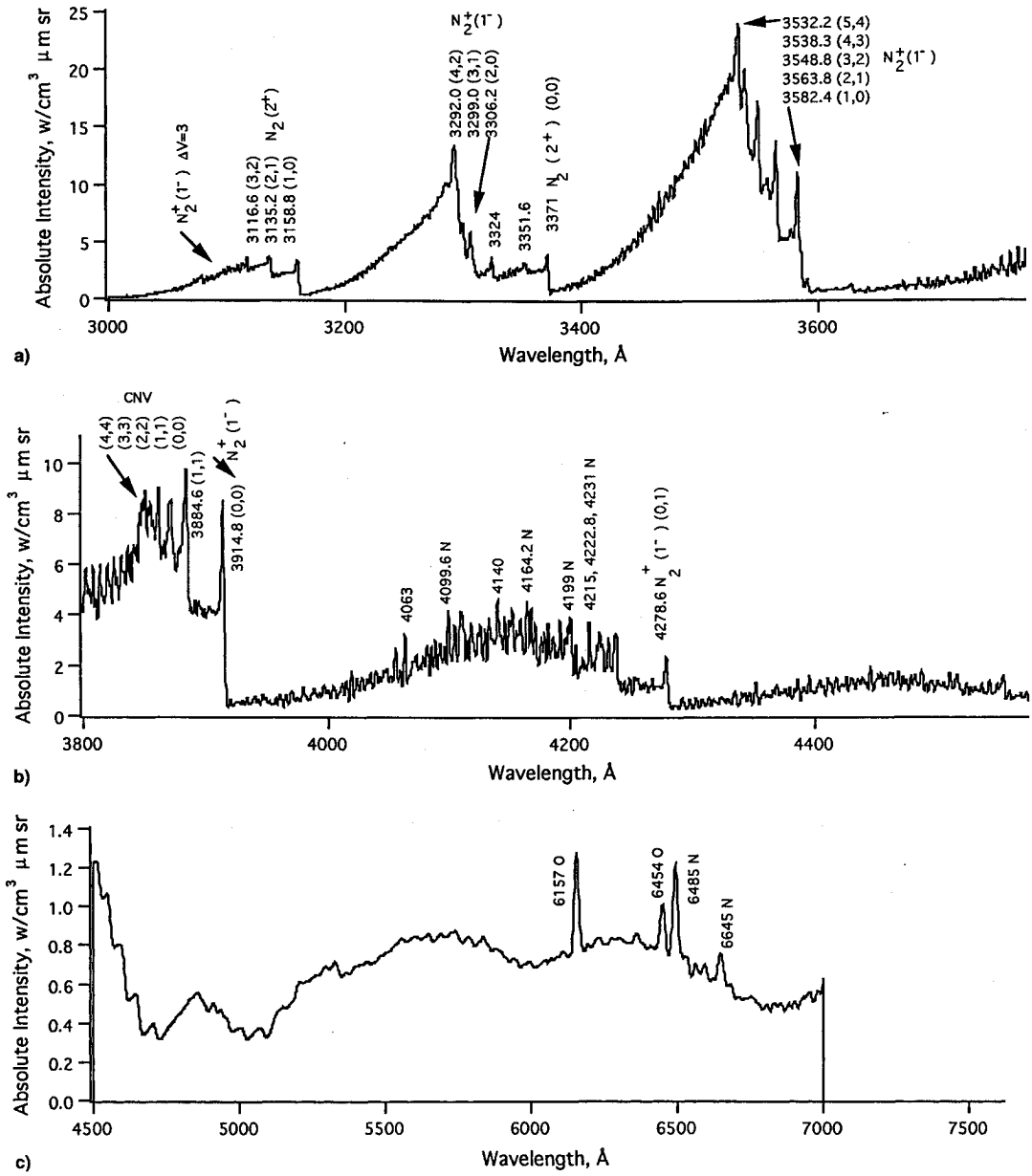

Fig. 9 Adjusted nonequilibrium synthetic spectrum. Point of peak radiation, spectral range a) 3000–3800, b) 3800–4600, and c) 4500–7000 Å.

2. Vibrational Factor F(v')

The vibrational expression was selected to be similar to the rotational expression because there is some indication in the data that the lower vibrational levels may be populated higher than that given by a Boltzmann distribution at a fixed vibrational temperature. Exploratory calculations indicated that holding the vibrational populations equal to the population of the $v' = 0$ level was unrealistic and gave an extremely high intensity for the $N_2^+(1^-)\Delta v = +1$ sequence. Thus, the intercept of the Gaussian on the $F(v')$ axis at $v' = 0$ was set equal to 1.0, and the peak value at $v' = v_p$ was determined in the following way.

The maximum population for any vibrational level is assumed to be the same as the population of the $v' = 0$ level, which would correspond to a vibrational temperature of infinity. Thus, a factor α is defined that gives the adjusted population of the v' level $\bar{n}(v')$ as a fraction of the way from the original population $n(v')$, to the maximum possible population $n(0)$. That is,

$$\bar{n}(v') = n(v') + \alpha[n(0) - n(v')] \tag{5}$$

When the values of α and v_p are specified, the value of $F(v') = F(v_p)$ at the peak of the Gaussian is given by

$$F(v_p) = (1.0 - \alpha) + \alpha[n(0)/n(v_p)] \tag{6}$$

$F(v')$ can now be found from expressions (2) and (4) given for $F(N')$ except, of course, that v' is substituted for N'.

C. Computed Spectra After Adjustments

The computed spectra after making the adjustments as previously discussed are shown in Figs. 8 and 9. Clearly, the agreement with the experimental data is now quite good. However, for the steady-state region (and certainly for an actual equilibrium region) it would be unrealistic to adjust the species concentration or level population without changing the temperature. The fact that we must change some level populations to agree with the data clearly indicates, as previously noted, that the shock-tube flow may be in a steady state at $x = 2.21$ cm behind the shock wave, but it is not in equilibrium. Some of the difference may be because of radiative cooling, which is not included in the calculations.

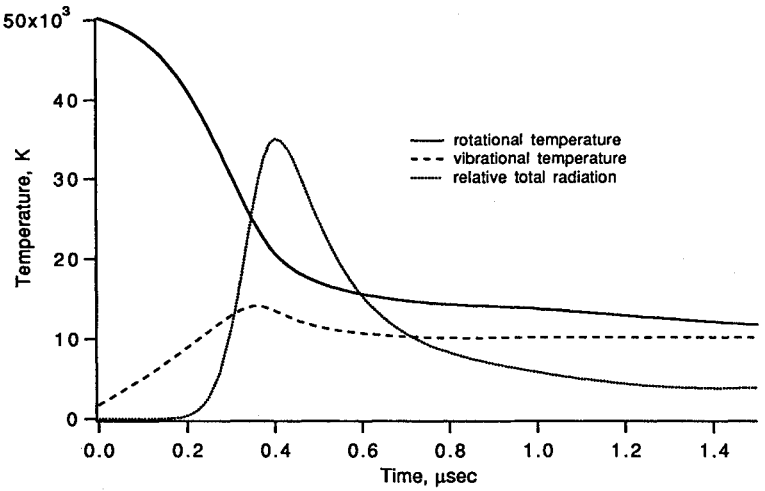

Fig. 10 Rotational and vibrational temperatures as functions of time.

VI. Discussion of Models

A. QSS Formulation

The fact that the results were unaffected by setting the escape factor to either 1.0 or 0.0, indicates that there may be a problem with the lumping of several electronic states into a single composite state for ease of QSS computations. The effect of the excitation rates and radiative rates on individual levels may differ substantially from the average effects over a composite state.

The upper state populations are calculated using the QSS formalism, which has been proven to be of enormous value. However, the present implementation of this method has some severe limitations. Atoms typically have several hundred energy levels below the first ionization level and a few others above this level. The present QSS code, as noted previously, lumps many of these levels into composite levels to reduce the effort required to produce the excitation data file and the computer time required to run the code. For example, the first five levels of atomic N are used explicitly and the others are lumped into 17 composite levels. For atomic O, the first seven levels are used explicitly and the others are lumped into 12 composite levels. The excitation array for N then contains 22 $\times$ 22 = 484 elements, each of which must contain all of the appropriate excitation and radiation cross section. As many (most) of these parameters are not known experimentally, they are usually calculated from empirical equations that fit theoretically produced values. It is not very clear how many electronic levels would be required to provide an acceptable accuracy. But it must be pointed out that the size of the required array elements in the computation matrix grows proportional to the square of the number of electronic states. For example, 100 electronic levels would require a 100 $\times$ 100 array, and that would involve 10,000 array elements!

The QSS situation for diatomic molecules is in a more difficult position than for atoms. There are about as many molecular electronic states as there are atomic states, but most of them lie at very high energy levels and are not needed in the QSS formalism to estimate the populations of the lower states. Presently, only 3–5 electronic energy states are included in the QSS code. Such a simplified procedure cannot be expected to predict accurately all of the effects of an enormously complex process.

The $N_2^+(1^-)$ band system, whose radiant intensity was predicted quite accurately for the steady-state conditions, and was only a factor of 3 too high for the nonequilibrium conditions, involves transitions between the second excited state ($B^2\Sigma_u^+$ state) and the ground state ($X^2\Sigma_g^+$ state). The upper state is only 25,460 cm^{-1} above the ground state and nearly 50,000 cm^{-1} below the dissociation level of the ground state. These conditions probably give the limited QSS procedure used the best opportunity to produce reasonable results.

The cases for the $N_2(1^+)$ and $N_2(2^+)$ band systems are not so ideal. Both of these transitions are from an upper excited state to a lower excited state, where the upper states are near the dissociation energy of the ground state. For example, the upper state of the $N_2(2^+)$ band system ($C^3\Pi_u$) is actually 10,422 cm^{-1} above the dissociation energy. Further, there are 11 electronic states of lower energy and at least 10 other nearby states of slightly higher energy. The calculation of a reliable population for this state might require as many as 20 states in the QSS formulation.

B. Temperatures

The effective rotational and vibrational temperatures as calculated by the flow code are shown in Fig. 10. The total radiation in arbitrary units as seen by a PMT is also plotted in the figure, as a locator of the points of peak nonequilibrium radiation and steady-state radiation. Interpreting the population ratios as temperatures has little physical meaning, but it does provide a comfortable intuitive picture of the trend caused by increasing or decreasing the populations.

In the flow code the rotational temperature is set equal to the translational temperature. However, from Fig. 7 it can be easily seen that the resultant rotational temperature at the point of peak radiation needed to fit the data exceeds the translational temperature from the flow code. A low calculated translational temperature is a possibility. Presently, the calculated translational temperature immediately behind the shock wave is less than the full Rankine–Hugoniot temperature, as some adjustment of the internal energy of the gas is allowed. Other factors that may affect the calculated vibrational and rotational temperatures are the radiative cooling, as previously noted, and the nonequilibrium population distribution. An evaluation of these effects is currently being explored by using an iterative process.

VII. Summary

The GENRAD code, a modified version of the NEQAIR code, which incorporates a radiation model based on our present understanding of nonequilibrium phenomena, tends to overpredict the intensities of many atomic O and N lines, and underpredicts the intensity of the $N_2(2^+)$ band system. The plateau in the total radiation trace, historically termed an equilibrium region, does not represent a true equilibrium regime. Some electronic states still remain in nonequilibrium in this region, and therefore, at best, this plateau may be referred as a steady-state regime. The code predicts the intensity of the $N_2^+(1^-)$ band system for the steady-state regime reasonably well, and for the nonequilibrium regime within a factor of 2–

3. However, the experiments show that in the nonequilibrium region, the upper states of various atomic transitions are overpopulated by the code and that the rotational and vibrational populations are not described by a Boltzmann distribution.

After some arbitrary adjustments in the electronic state populations and the distribution of rotational and vibrational populations, it was possible to match the calculated data with the experiments. From this exercise it appears that, for correct modeling, the QSS formulations must be expanded to include a more individual level, as opposed to combining several densely packed electronic levels into one composite level. However, in doing so, the computational size of the problem will increase as the square of the number of electronic energy levels. Radiative cooling may also be playing a role in reducing the upper state populations by reducing the electron temperature. This aspect requires further investigation.

References

[1]Allen, R. A., Rose, P. H., and Camm, J. C., "Nonequilibrium and Equilibrium Radiation at Super-Satellite Re-Entry Velocities," AVCO Everett Research Lab., Research Rept. 156, Everett, MA, Sept. 1962.

[2]Teare, J. D., Georgiev, S., and Allen, R. A., "Radiation from the Nonequilibrium Shock Front," AVCO Everett Research Lab., Research Rept. 112, Everett, MA, Oct. 1961.

[3]Camm, J. C., Kivel, R. L., Taylor, R. L., and Teare, J. D., "Absolute Intensity of Nonequilibrium Radiation in Air and Stagnation Heating at High Altitudes," AVCO Everett Research Lab., Research Rept. 93, Everett, MA, Dec. 1959.

[4]Sharma, S. P., and Gillespie, W. D., "Nonequilibrium and Equilibrium Shock Front Radiation Measurements," *Journal of Thermophysics and Heat Transfer*, Vol. 5, No. 3, 1991, pp. 257–265; also AIAA Paper 90-0139, Jan. 1990.

[5]Sharma, S. P., Gillespie, W. D., and Meyer, S. A., "Shock Front Radiation Measurements in Air," AIAA Paper 91-0573, Jan. 1991.

[6]Howe, J. T., "Introductory Aerothermodynamics of Advanced Space Transportation Systems," *Journal of Spacecraft and Rockets*, Vol. 22, No. 1, 1985, pp. 19–26.

[7]Park, C., "Calculation of Nonequilibrium Radiation in the Flight Regimes of Aeroassisted Orbital Transfer Vehicles," *Thermal Design of Aeroassisted Orbital Transfer Vehicles*, edited by H. F. Nelson, Vol. 96, Progress in Aeronautics and Astronautics, AIAA, New York, 1985, pp. 395–418.

[8]Park, C., "Radiation Enhancement by Nonequilibrium in Earth's Atmosphere," *Journal of Spacecraft and Rockets*, Vol. 22, No. 1, 1985, pp. 27–36; also AIAA Paper 83-0410, Jan. 1983.

[9]Page, W. A., and Arnold, J. O., "Shock Layer Radiation of Blunt Bodies at Entry Velocities," NASA TR R-193, April 1964.

[10]Seiff, A., Reese, D. E., Sommer, S. C., Kirk, D. B., Whiting, E. E., and Niemann H. B., "PAET, an Entry Probe Experiment in the Earth's Atmosphere," *Icarus, International Journal of the Solar System*, Vol. 18, No. 4, 1973, pp. 525–563.

[11]Cauchon, D. L., "Project Fire Flight 1 Radiative Heating Experiment," NASA TM X-1222, April 1966.

[12]Cauchon, D. L., "Radiative Heating Results from the Fire 2 Flight Experiment at a Reentry Velocity of 11.4 Kilometers per Second," NASA TM X-1402, July 1967.

[13]Lee, D. B., and Goodrich, W. D., "The Aerothermodynamic Environment of the Apollo Command Module During Super-Orbital Entry," NASA TN D-6792, April 1972.

[14]Curry, D. M., and Stephens, E. W., "Apollo Ablator Thermal Performance at Super-Orbital Entry Velocities," NASA TN D-5969, Sept. 1970.

[15]Shirai, H., and Park, C., "Experimental Studies of Radiative Base Heating of a Jovian Entry Model," *Entry Heating and Thermal Protection*, edited by W. B. Olstad, Vol. 69, Progress in Astronautics and Aeronautics, AIAA, New York, 1980, pp. 148–171.

[16]Park, C., "Calculation of Radiation from Argon Shock Layers," *Journal of Quantitative Spectroscopy and Radiative Transfer*, Vol. 28, No. 1, 1982, pp. 29–40.

[17]Arnold, J. O., and Whiting, E. E., "Nonequilibrium Effects on Shock-Layer Radiometry During Earth Entry," *Journal of Quantitative Spectroscopy and Radiative Transfer*, Vol. 13, No. 9, 1973, pp. 861–870.

[18]Cooper, D. M., Jaffe, R. L., and Arnold, J. O., "Computational Chemistry and Aeroassisted Orbital Transfer Vehicles," *Journal of Spacecraft and Rockets*, Vol. 22, No. 1, 1985, pp. 60–67.

[19]Menees, G. P., "Thermal-Protection Requirements for Near-Earth Aeroassisted Orbital-Transfer Vehicle Missions," AIAA Paper 83-1513, June 1983.

[20]Park, C., "Comparison of Electron and Electronic Temperatures in Recombining Nozzle Flow of Ionized Nitrogen-Hydrogen Mixture: Part 2—Experiments," *Journal of Plasma Physics*, Vol. 9, Pt. 2, 1973, pp. 217–234.

[21]Sharma, S. P., Huo, W. M., and Park, C., "The Rate Parameters for Coupled Vibration-Dissociation in a Generalized SSH Approximation," *Journal of Thermophysics and Heat Transfer*, Vol. 6, No. 1, 1992, pp. 9–21; also AIAA Paper 88-2714, June 1988.

[22]Sharma, S., "Vibrational and Rotational Temperature Measurements in a Shock Tube," 18th International Symposium on Shock Waves, Sendai, Japan, July 1991.

[23]Sharma, S. P., "Assessment of Nonequilibrium Radiation Computation Methods for Hypersonic Flows," *International Journal of Modern Physics C*, Vol. 4, No. 4, 1993, pp. 847–881; also NASA TM 103994, Jan. 1993.

[24]Park, C., *Nonequilibrium Hypersonic Aerothermodynamics*, Wiley, New York, 1990.

[25]Whiting, E. E., and Park, C., "Radiative Heating at the Stagnation Point of the AFE Vehicle," NASA TM 102829, Nov. 1990.

[26]Moreau, S., Laux, C. O., Chapman, D. R., and MacCormack, R. W., "A More Accurate Nonequilibrium Air Radiation Code: NEQAIR Second Generation," AIAA Paper 92-2968, July 1992.